AD A089413

REPORT DOCUMENTATION PAGE		READ INSTRUCTIONS BEFORE COMPLETING FORM
1. REPORT NUMBER AFOSR TR-80-0945	2. GOVT ACCESSION NO. AD-A089413	3. RECIPIENT'S CATALOG NUMBER
4. TITLE (and Subtitle) ON THE CORRELATION STRUCTURE OF NEAREST NEIGHBOR RANDOM FIELD MODELS OF IMAGES.		5. TYPE OF REPORT & PERIOD COVERED Interim rept.
		6. PERFORMING ORG. REPORT NUMBER
7. AUTHOR(s) R. Chellappa		8. CONTRACT OR GRANT NUMBER(s) AFOSR-77-3271
9. PERFORMING ORGANIZATION NAME AND ADDRESS University of Maryland Computer Science Center College Park, MD 20742		10. PROGRAM ELEMENT, PROJECT, TASK AREA & WORK UNIT NUMBERS 61102F 2304/A2
11. CONTROLLING OFFICE NAME AND ADDRESS Air Force Office of Scientific Research/NM Bolling AFB, Washington, DC 20332		12. REPORT DATE July 1980
		13. NUMBER OF PAGES 56
14. MONITORING AGENCY NAME & ADDRESS(if different from Controlling Office) TR-912		15. SECURITY CLASS. (of this report) UNCLASSIFIED
		15a. DECLASSIFICATION DOWNGRADING SCHEDULE

16. DISTRIBUTION STATEMENT (of this Report)

Approved for public release; distribution unlimited.

17. DISTRIBUTION STATEMENT (of the abstract entered in Block 20, if different from Report)

DISTRIBUTION STATEMENT A
Approved for public release;
Distribution Unlimited

ACCESSION for
NTIS   White Section ☑
DDC   Buff Section ☐
UNANNOUNCED   ☐
JUSTIFICATION

BY
DISTRIBUTION/AVAILABILITY CODES
Dist.   AVAIL. and/or SPECIAL

A

18. SUPPLEMENTARY NOTES

19. KEY WORDS (Continue on reverse side if necessary and identify by block number)

Image processing
Random fields
Autocorrelation

20. ABSTRACT (Continue on reverse side if necessary and identify by block number)

This paper discusses the correlation structure of some two-dimensional nearest neighbor random field models of images. The correlation structure of two non-equivalent random field models, the so-called simultaneous model and the conditional Markov model, are analyzed incontinuous as well as discrete space. Analyses of two-dimensional moving average models and autoregressive and moving average models are also included. Based on the structure of the correlation function at lower lags an empirical test is suggested for the inference of image models. Examples from real textures are given.

DD FORM 1473   EDITION OF 1 NOV 65 IS OBSOLETE
1 JAN 73
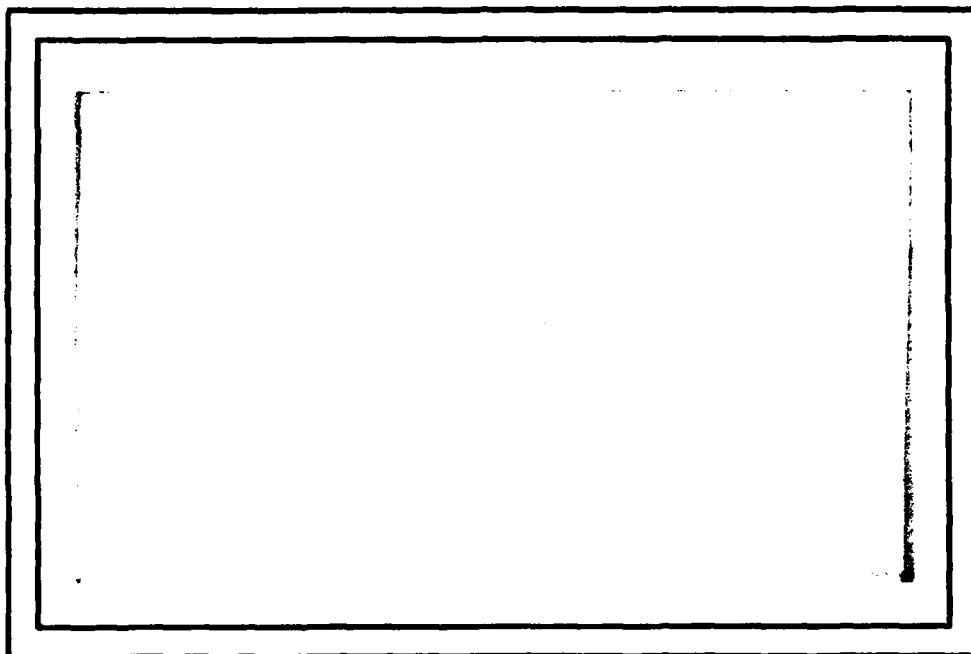411074

AD A089413

UNIVERSITY OF MARYLAND

COMPUTER SCIENCE CENTER

COLLEGE PARK, MARYLAND
20742

80 9 22 111

TR-912
AFOSR-77-3271

July, 1980

ON THE CORRELATION STRUCTURE
OF NEAREST NEIGHBOR
RANDOM FIELD MODELS OF IMAGES

R. Chellappa
Computer Vision Laboratory
Computer Science Center
University of Maryland
College Park, MD 20742

ABSTRACT

This paper discusses the correlation structure of some two-dimensional nearest neighbor random field models of images. The correlation structure of two nonequivalent random field models, the so-called simultaneous model and the conditional Markov model, are analyzed in continuous as well as discrete space. Analyses of two-dimensional moving average models and autoregressive and moving average models are also included. Based on the structure of the correlation function at lower lags an empirical test is suggested for the inference of image models. Examples from real textures are given.

1. Introduction

Random field (RF) models have many applications in image processing and analysis. Typically, an image is represented by a two-dimensional scalar array, the gray level variations defined over a grid. One of the important characteristics of this data is the statistical dependence of the gray levels within a neighborhood. For example, $y(s_1,s_2)$, the scalar gray level at position (s_1,s_2), might be statistically dependent on the values of gray levels over a neighborhood that includes $\{(s_1-1,s_2), (s_1+1,s_2), (s_1,s_2-1), (s_1,s_2+1)\}$. This is in contrast to the familiar time series models where the dependence is strictly on the past observations. An image represents a statistical phenomenon on a plane and hence the notion of past and future as understood in classical time series analysis is not relevant.

Prior to the use of RF models for images, one of the basic problems to be tackled is the choice of an appropriate model. Suppose we are given a set of observations $\{y(s), s \in \Omega\}$, $\Omega = \{s = (i,j), 1 \leq i,j \leq M\}$, defined over a square lattice and it is required to identify an appropriate two-dimensional RF model to fit the given data. In such situations not only do we have all the usual problems of model specification that arise in time series analysis but in addition we have problems that arise from the possible existence of directionality of dependence. Even when only the 8 nearest neighbors are allowed there are 2^8 possible neighbor sets to be considered. If some inference regarding

directionality of dependence can be made, many savings can be achieved in the search for appropriate models.

Secondly, the neighbor set selection procedure developed in [1] assumes that a basic set of "good models" is available and chooses the best model from the given set. Usually, the basic set of "good models" is chosen by intuition or by using some ideas regarding the underlying physical processes that might have generated the data. As it is often difficult to understand the underlying physical processes, some empirical tools are necessary to make a reasonable choice of good models.

In this paper we suggest some empirical methods using the autocorrelation function (ACF) for the inference of a basic set of two-dimensional RF models. Such methods are quite popular in time series analysis [2]. For instance, if the sample ACF of the given one-dimensional (weakly stationary) time series is very small after a few lags (say) p, then one might use a moving average model of order p. The ACF is a useful tool in the inference of basic models since it together with the mean and variance possesses all the information about the underlying probability distribution under a Gaussian assumption. It might be expected that such methods should find use in inferences regarding two-dimensional RF models.

We first analyze the correlation structure of two-dimensional RF models and subsequently discuss their use in the inference of models.

We consider three different classes of two-dimensional RF models, the simultaneous models [3-6], the conditional Markov models [4,6-7], and the moving average (MA) and the autoregressive and moving average (ARMA) models. Our main concern is focussed on the so-called nearest neighbor (NN) modes, i.e. the dependence is restricted to the 8 neighbors. The three classes of models mentioned above are non-equivalent. For a given simultaneous model an equivalent (in second order properties) conditional Markov model can always be found but the converse is not true. The underlying probability structures of the NN simultaneous models and NN conditional models are different. The conditional expectation $E(y(s)|\text{all } y(s_1), s_1 \in \Omega, s_1 \neq s)$ depends only on the members of the neighbor set of dependence for the conditional models, but this is not true for the simultaneous models. The class of spatial MA models falls outside the classes of finite simultaneous and conditional models and seems to be of a basically different structure.

The ACF can be used in two ways for the inference of models. First by matching the numerical values of the theoretical ACF for different models and the sample estimate of ACF, useful inferences may be drawn. This assumes the availability of theoretical ACFs for the different models mentioned above. The expressions for the ACF can be written down easily for spatial moving average models and simultaneous RF models with unilateral or causal neighbor set dependence as in [8]. When bilateral dependence is introduced along either or both of the

axes, the recursive method used in [8] is not applicable. How-
ever the ACF can be computed for both simultaneous models and
conditional Markov models for any arbitrary neighborhood by
using RF representations on torus lattices [6].

Secondly, the specific structure of the ACF at lower lags,
viz., whether it is convex downwards or concave downwards, can
be used in making additional inferences about the model. This
can be understood by considering the ACFs of spatial and temporal
autoregressions in the one-dimensional case. It is well known
that the ACF $R(t)$ for a stationary Gaussian Markov process depends
on distance and is given by $R(t) = e^{-\alpha t}$, $t \geq 0$, where α is some
constant. This function is downward convex to the right of the
origin (i.e. $\frac{d}{dt}R(t)\big|_{t=0} < 0$). Consider the spatial autoregression

$$x_t = a(x_{t-1} + x_{t+1}) + u_t \qquad (1.1)$$

Using the central difference operator (1.1) can be written as

$$(1-2a)x_t = a\Delta^2 x_t + u_t \qquad (1.2)$$

where Δ^2 is the second order central difference operator. Now,
consider the continuous analog of (1.2), namely

$$(\frac{d^2}{dv^2} - \gamma^2)x(v) = u(v) \qquad (1.3)$$

where $\gamma^2 = (1-2a)/a$. The ACF for this model can be shown to be
[9]

$$R(v) = (1+\gamma v)e^{-\gamma v} \qquad (1.4)$$

and $\frac{d}{dv} R(v)\big|_{v=0} = 0$. The spatial autoregression possesses an ACF
that is downward concave at the origin, unlike the Gaussian-Markov

processes, and it appears that directionality can be inferred by studying the behavior of the low-order correlation structure. Similar behavior of the ACF for continuous RF models has been noted in the literature [3]. Thus in the two-dimensional continuous case, depending on whether or not bilateral dependence is introduced along the axes, concave (flat) or convex (nonflat) behavior is noted. Using a discrete equivalent of the nonflat / flat condition, inferences about the directionality can be made, for the discrete RF models.

Our approach to the analysis of ACF structure is as follows:

We first consider the structure of the ACF of continuous RF models corresponding to discrete simultaneous and conditional models. The former models yield linear two-dimensional stochastic partial differential equations (SPDE) while the latter correspond to a spatial temporal model. By identifying the appropriate Green's functions the flat/nonflat structure of the ACF is analyzed and a case is established for its use in the inference of models.

Using the RF representations on torus lattices we compute the ACFs for different neighbor sets for the discrete simultaneous and conditional models and analyze their structure. Some of the interesting observations are: (1) The simultaneous models have high correlation values compared to the conditional models for the same neighbor set and parameter values. (2) When bilateral dependence is introduced the NN simultaneous models exhibit a flat structure along the axes for certain ranges of parameter

values. For instance, when the isotropic dependence is on the east, west, north, and south neighbors, flat structure along the i,j axes is observed, followed by flat structure along the i,j,k axes (see Fig. 1) as the parameter value is increased. (3) The NN conditional models do not exhibit flat structure for the same neighbor set of dependence and parameter values as in the simultaneous models.

To check whether real image patterns exhibit flat/nonflat behavior, experiments were performed with texture and terrain samples. The sample ACFs of 64x64 windows were computed and the ACF structures at lower lags were examined. The samples of sand, grass, and wool exhibit flat structure along all axes, while the samples of raffia exhibit flat structure only along the i and j axes. On the other hand, the sampes of Lower Pennsylvanian shale and Mississippian limestone and shale exhibit nonflat structure in all directions. The samples of Pennsylvanian sandstone and shale exhibit flat structure along the i axis alone and nonflat structure along the other two axes.

The organization of the paper is as follows: Sections 2 and 3 consider the correlation structures of continuous and discrete RF models respectively. In Section 4, experimental results with real texture images are given. By matching the sample ACF and theoretical ACF, inferences regarding the appropriate model are given. Discussion is given in Section 5.

2. Correlation structure of continuous random fields

In this section we begin with discrete, two-dimensional RF models, consider their continuous counterparts, and discuss the correlation structure of the continous RF models. Simultaneous RF models are classified as causal models (unilateral dependence along i,j), semicausal models (unilateral along j and bilateral along i), and noncausal models (bilateral along i and j). The continuous equations corresponding to these models are hyperbolic, parabolic, and elliptic SPDE [10], respectively. The continuous model corresponding to the conditional Markov model with neighbor set dependence on the east, west, north, and south is a spatial-temporal model [4]. By constructing the Green's function using transform techniques [11] the ACF is derived for each of these models.

It turns out that the ACF of the hyperbolic equation is nonflat along all directions; that of the parabolic equation is flat along the i axis and nonflat along the j axis; that of the elliptic equation is flat along all directions; and that corresponding to the spatial temporal model mentioned above is nonflat along all axes. Based on these observations a prima facie case is established for using the structure of the ACF for drawing inferences about RF models.

We first establish some framework for the computation of the ACF of an SPDE [12] and consider the different cases separately. Consider the general second-order linear SPDE

$$\left(a\,\frac{\partial^2}{\partial x^2} + b\,\frac{\partial^2}{\partial y^2} + 2h\,\frac{\partial^2}{\partial x \partial y} + 2g\,\frac{\partial}{\partial x} + 2f\,\frac{\partial}{\partial y} + c\right)$$

$$u(x,y) = \varepsilon(x,y) \qquad (2.1)$$

or equivalently

$$P\left(\frac{\partial}{\partial x}, \frac{\partial}{\partial y}\right) u(x,y) = \varepsilon(x,y) \qquad (2.2)$$

where P is the polynomial in $\frac{\partial}{\partial x}, \frac{\partial}{\partial y}$ and $\varepsilon(\cdot)$ is uncorrelated noise, with zero mean and variance σ^2. The solution to (2.2) can be written as

$$u(x,y) = \int_{-\infty}^{\infty} \int_{-\infty}^{\infty} G(x-u, y-v)\,\varepsilon(u,v)\,du\,dv \qquad (2.3)$$

where $G(x,y)$ is the Green's function satisfying

$$P\left(\frac{\partial}{\partial x}, \frac{\partial}{\partial y}\right) G(x,y) = \delta(x,y) \qquad (2.4)$$

and

$$\delta(x,y) = 1 \qquad \text{if } x = y = 0$$
$$= 0 \qquad \text{otherwise}$$

When $\varepsilon(u,v)$ are entirely uncorrelated random impulses, we have for the autocorrelation of the process $u(x,y)$,

$$\text{cor}_u(x,y) = \sigma^2 \int_{-\infty}^{\infty} \int_{-\infty}^{\infty} G(u,v)\,G(u-x, v-y)\,du\,dv$$

and the normalized correlation function of $u(x,y)$ is

$$\rho(x,y) = \frac{\displaystyle\int_{-\infty}^{\infty} \int_{-\infty}^{\infty} G(u,v)\,G(u-x, v-y)\,du\,dv}{\displaystyle\int_{-\infty}^{\infty} \int_{-\infty}^{\infty} G^2(u,v)\,du\,dv} \qquad (2.5)$$

Case i: (Hyperbolic)

Consider the causal or unilateral RF model

$$y(i,j) + \theta_1 y(i,j-1) + \theta_2 y(i-1,j) + \theta_3 y(i-1,j-1) = \sqrt{\nu}\,\omega(i,j) \qquad (2.6)$$

where $\omega(i,j)$, $(i,j) \in \Omega$, is an independent and identically distributed zero mean, unit variance noise sequence. When $\theta_3 = \theta_1 \theta_2$, we obtain the popular separable model widely used in the image processing literature [13].

The continuous counterpart of (2.6) is

$$(\frac{\partial^2}{\partial x \partial y} + a_1 \frac{\partial}{\partial x} + a_2 \frac{\partial}{\partial y} + a_3) u(x,y) = \epsilon(x,y) \qquad (2.7)$$

When $a_3 = a_1 a_2$, we obtain a separable hyperbolic equation. The Green's functiion $G(x,y)$ corresponding to (2.8) can be written as [11]

$$G(x,y) = e^{-a_2 x - a_1 y} J_0(2\sqrt{(a_3 - a_1 a_2) xy})\, u(x)u(y) \qquad (2.8)$$

where $J_0(\cdot)$ is the Bessel function of the first kind and zeroth order and $U(\cdot)$ is the unit step function. As the resulting ACF structure is tedious to analyze we consider the separable model, i.e., $a_3 = a_1 a_2$. Using this assumption and $J_0(0) = 1$, we have

$$G(x,y) = e^{-a_2 x - a_1 y} u(x)u(y) \qquad (2.9)$$

Substituting (2.9) in (2.5)

$$\rho(x,y) = \exp(-\alpha|x| - \alpha|y|) \qquad (2.10)$$

Before proceeding further we give a formal definition of the flat/nonflat structure.

Definition: The ACF is flat along the x axis if $\dfrac{\partial(x,y)}{\partial x}\Big|_{x=0} = 0$ and

is nonflat if $\dfrac{\partial(x,y)}{\partial x} < 0$ to the right of the origin, i.e.,

$\dfrac{\partial(x,y)}{\partial x}\Big|_{x=\xi} < 0$, for $\xi > 0$ and arbitrarily close to the origin.

(This particular definition of nonflat structure is used to get

over some singularities at the origin.)

From the definition and eq. (2.10) it is clear that the

ACF for the hyperbolic case is nonflat along the x and y direc-

tions.

Case ii: (Parabolic)

Consider the semicausal model

$$y(i,j) = a(y(i-1,j) + y(i+1,j) + y(i,j-1)) + \sqrt{\nu}\,\omega(i,j) \quad (2.11)$$

where $|a| < \dfrac{1}{3}$ to ensure stationarity and $\omega(i,j)$ is as in eq. (2.6).

Eq. (2.11) can be written as

$$y(i,j)-3ay(i,j) = a\{y(i-1,j)+y(i+1,j)-2y(i,j)$$
$$- y(i,j)-y(i,j-1)\} + \omega(i,j)$$

Using the continuous approximation we have the parabolic

equation

$$(\frac{\partial}{\partial y} - \frac{\partial^2}{\partial x^2} + \gamma^2)u(x,y) = \varepsilon(x,y) \qquad (2.12)$$

where $\gamma^2 = (1-3a)/a$.

The Green's function corresponding to this equation can be

written as [11]

$$G(x,y) = \frac{1}{2\sqrt{\pi y}} \exp(-\gamma^2 y - \frac{x^2}{4y})u(y) \qquad (2.13)$$

Eqn. (2.13) shows that an impulse at the origin only has an effect at positive values of y. Thus the y axis is a time-like axis whereas the x-axis is a space-like axis. Substituting (2.13) in (2.5) (we are omitting the manipulation details), the ACF is

$$\rho(x,y) = e^{-\gamma x}\phi\left(\frac{x}{\sqrt{2y}} - \gamma\sqrt{2y}\right) + e^{\gamma x}\left(1-\phi\left(\frac{x}{\sqrt{2y}} + \gamma\sqrt{2y}\right)\right) \qquad (2.14)$$

where $\phi(x)$ is the probability that a standardized Gaussian random variable X is $\leq x$.

We now show that $\rho(x,y)$ in (2.14) is flat along the x-axis and nonflat along the y-axis. Differentiating (2.14) w.r.t. x,

$$\frac{\partial\rho(x,y)}{\partial x} = -\gamma e^{-\gamma x}\phi\left(\frac{x}{\sqrt{2y}} - \gamma\sqrt{2y}\right) + e^{-\gamma x}\phi\frac{\partial}{\partial x}\left(\frac{x}{\sqrt{2y}} - \gamma\sqrt{2y}\right)$$

$$+ \gamma e^{\gamma x}\left(1-\phi\left(\frac{x}{\sqrt{2y}} + \gamma\sqrt{2y}\right)\right) - e^{-\gamma x}\frac{\partial}{\partial x}\phi\left(\frac{x}{\sqrt{2y}} - \gamma\sqrt{2y}\right) \qquad (2.15)$$

Since $\phi(b(x)) = \frac{1}{\sqrt{2\pi}}\int_{-\infty}^{b(x)} e^{-t^2/2}dt$

$$\frac{\partial\phi}{\partial x}(b(x)) = \frac{1}{\sqrt{2\pi}}e^{-\frac{(b(x))^2}{2}}\frac{db(x)}{dx} \qquad (2.16)$$

Using (2.16) and $\phi(-x) = 1-\phi(x)$ we have $\frac{\partial\rho}{\partial x}(x,y)\Big|_{x=0} = 0$

Similarly, differentiating with respect to y, it can be shown that

$$\frac{\partial\rho(x,y)}{\partial y} = -\frac{\gamma}{\sqrt{\pi}}\exp\left(-\frac{x^2}{4y} - \gamma^2 y\right)/y^{1/2}$$

which by definition is not flat along the y axis.

Case iii (Elliptic):

Consider the discrete model

$$y(i,j) = a(y(i,j-1)+y(i,j+1)+y(i-1,j)+y(i+1,j))+\sqrt{\nu}\omega(i,j) \quad (2.17)$$

Proceeding similarly to the parabolic case, the continuous counterpart of (2.17) is

$$(\frac{\partial^2}{\partial x^2} + \frac{\partial^2}{\partial y^2} - \alpha^2)u(x,y) = \iota(x,y) \quad (2.18)$$

where $\alpha^2 = (1-4a)/a$

The Green's function for this equation is [3]

$$G(s) = \frac{1}{2\pi} K_0(\alpha s) \quad (2.18)$$

where $s = \sqrt{x^2+y^2}$ and $K_0(\cdot)$ is the modified Bessel function of the second kind. Substituting (2.18) in (2.5), the ACF for the elliptic case is

$$\rho(s) = (\alpha s)K_1(\alpha s) \quad (2.19)$$

Both the axes are space-like and the function $\rho(s)$ is flat in all directions.

Case iv (Conditional Markov):

Consider the isotropic conditional model where the observation at (i,j) depends on the east, west, north, and south neighbors. The basic equation of this model is

$$E(y(s)|all\ y(s_1),\ s_1 \in \Omega,\ s_1 \neq s)$$
$$= \beta[y(s+(i-1,j))+y(s+(i+1,j))+y(s+(i,j-1))+y(s+(i,j+1))] \quad (2.20)$$

Equivalently, (2.20) can be written as

$$y(i,j) = \beta[y(i-1,j)+y(i+1,j)+y(i,j-1)+y(i,j+1)]+\sqrt{\nu}\eta(i,j) \quad (2.21)$$

where $\eta(i,j)$, $(i,j) \in \Omega$ is a correlated noise sequence with zero mean and variance unity. In the Gaussian case, it can be shown [4] that the spectral density function of the RF model in (2.21) is similar to the marginal spectrum of a spatial temporal model,

$$dy_{i,j,t} = -\lambda \Psi(E) y_{i,j,t} dt + dz_{i,j,t} \tag{2.22}$$

where

$$(\Psi(E)-1) y_{i,j} = \beta (y_{i-1,j} + y_{i+1,j} + y_{i,j-1} + y_{i,j+1}) \tag{2.23}$$

and $dz_{i,j,t}$ are homogeneous <u>independent</u> terms with zero mean.

In the limiting case, the continuous counterpart of (2.22), (2.23) is

$$[\frac{\partial}{\partial t} + k^2 - (\frac{\partial^2}{\partial x^2} + \frac{\partial^2}{\partial y^2})] u(x,y) = z(x,y) \tag{2.24}$$

which is the well known diffusion equation. An appropriate Green's function [11] for (2.24) is

$$G(x,y,t) = \frac{1}{4\pi t} \exp\{-k^2 t - \frac{x^2+y^2}{4t}\}, \quad t > 0 \tag{2.25}$$
$$= 0, \text{ otherwise}$$

For this case, we have the covariance function

$$R(x,y) = \int_{\tau=0}^{\infty} \int_{u=-\infty}^{\infty} \int_{v=-\infty}^{\infty} G(u,v,\tau) G(u-x,v-y,\tau) du dv d\tau \tag{2.26}$$

Substituting (2.25) in (2.26) and performing the integration with respect to u,v co-ordinates (the manipulative details are omitted),

$$R(s) = \int_{t=0}^{\alpha} \frac{1}{t} \exp\{-2k^2 t - \frac{s^2}{8t} \, dt\}$$

$$= \frac{1}{4\pi} K_0(ks), \quad s = \sqrt{x^2 + y^2} \tag{2.27}$$

where K_0 is the modified Bessel function of the second kind.
For small values of s, $K_0(s)$ behaves like $-\ell ns$ and hence $R(s)$
is nonflat along all axes. (Note that since $K_0(s)$ is $-\infty$ at $s=0$,
we have avoided discussing the normalized ACF $\rho(s)$.

3. Correlation structure of discrete random fields

In the preceding section the flat/nonflat structure of the
ACFs for the continuous RF models was analyzed.   It is a natural
question to ask if such behavior is exhibited in the discrete
space.   To analyze the structure of the lattice ACFs we need to
obtain expressions for the correlation values for different
models, _viz._, the causal, semicausal, and noncausal simultaneous
models, the noncausal conditional Markov models, and the MA models.
The ACF for the causal neighbor set can be easily obtained by
using the recursive method [8].   This approach is not valid when
a bilateral dependence is introduced along any of the axes.   An
alternate procedure would be to consider the corresponding
spectral density function in the discrete space and use numerical
integration techniques to obtain the ACF.   This procedure becomes
tedious for different neighbor sets and also the resulting numer-
ical values are only approximate.

To compute the ACF for simultaneous and conditional models
for different neighbor sets we use RF representations on torus
lattices.   Such representations for conditional Markov models
have been suggested in [6,7] and for simultaneous models in
[5,6].   The advantage of the torus representation is that the
expressions for the ACF can be written in closed form for an
arbitrary neighbor set.   For large values of M, the edge effects
due to the torus representation can be ignored.

We first consider the ACF for causal neighbor sets defined on a plane lattice and then consider semicausal and noncausal representations on torus lattices. Our interest is not only to obtain the correlation values but also to analyze the flat/ nonflat structure at lower lags. The discrete equivalents of the criteria considered in Section 2 are defined below:

Definition: The discrete ACF $\rho(i,j)$ is flat along the i-axis if

$$1-\rho(1,0) < \rho(1,0)-\rho(2,0) \qquad (3.1)$$

flat along the j-axis if

$$1-\rho(0,1) < \rho(0,1)-\rho(0,2) \qquad (3.2)$$

and flat along the k-axis if

$$1-\rho(1,1) < \rho(1,1)-\rho(2,2) \qquad (3.3)$$

The ACF is nonflat along an axis if the reverse of the inequality is true.

3.1 Causal separable model

Consider the RF model

$$y(i,j) = \theta_{0,-1}y(i,j-1) + \theta_{-1,0}y(i-1,j) - \theta_{0,-1}\theta_{-1,0}y(i-1,j-1) + \sqrt{\nu}\,\omega(i,j) \qquad (3.4)$$

It is well known that the ACF is

$$\rho(i,j) = \theta_{-1,0}^{|i|}\theta_{0,-1}^{|j|}\,, \qquad |\theta_{0,-1}| < 1, |\theta_{-1,0}| < 1 \qquad (3.5)$$

Equation (3.1) requires

$$1-\theta_{-1,0} < \theta_{-1,0} - \theta_{-1,0}^2$$

$$\text{or} \quad (1-\theta_{-1,0}) < (1-\theta_{-1,0})\theta_{-1,0}$$

$$\text{or} \quad 1 < \theta_{-1,0}$$

which are not true due to the constraint on $\theta_{-1,0}$ in (3.5) to ensure stationarity. Similarly, it can be shown that the ACF is nonflat along the j and k axes.

To compute autocorrelations for neighbor sets with bilateral dependence, we use the RF representation on torus lattices which are defined below.

3.2 Simultaneous models on torus lattices

The basic equation is

$$y(s) - \delta = \sum_{(i,j) \in N} \theta_{i,j} \{y(s+(i,j)) - \delta\} = \sqrt{\nu}\,\omega(s), \quad s \in \Omega \qquad (3.6)$$

In (3.6), $\{\omega(s), s \in \Omega\}$ is a sequence of independent random variables with zero mean and unit variance. Note that $w(s)$ is correlated with $y(s+s_k)$ if the neighbor set includes bilateral dependence along any axis. The coefficients $\theta_{i,j}$ must satisfy the following condition to ensure homogeneity of the RF model:

$$\left| \sum_{(i,j) \in N} \theta_{i,j} z_1^i z_2^j \right| < 1 \quad \text{if } |z_1| = |z_2| = 1 \qquad (3.7)$$

Typical examples of neighbor sets N are

i) $\{(0,1),(1,0),(0,-1),(-1,0)\}$ (noncausal)

ii) $\{(1,0),(0,-1),(-1,0)\}$ (semicausal)

Note that the notation we use for indicating the neighbors is the same as the notation used in specifying Ω. The representation on torus lattices is introduced by imposing the condition

$$y[(i,j)+(i_1,j_1)] = y[(i+i_1-1)\bmod m+1, \ (j+j_1-1)\bmod m+1] \qquad (3.8)$$

for all $(i,j) \in \Omega$.

This particular representation leads to the following expression for the ACF:

$$\rho(k,\ell) \triangleq \mathrm{cov}[y(i_1,j_1), \ y(i_1+k, j_1+\ell)]$$

$$\approx \frac{\sum_{i,j=1} \lambda_0^{[i-1)k+(j-1)\ell]} / ||\mu_{ij}||^2}{\sum_{i,j=1}^{M} 1/||\mu_{ij}||^2} \qquad (3.9)$$

where

$$\mu_{ij} \triangleq 1 - \sum_{(m,n) \in N} \theta_{m,n} \lambda_0 [(i-1)k + (j-1)\ell], \qquad (3.10)$$

and $\lambda_0 = \exp\{\sqrt{-1} \; \frac{2\pi}{m}\}$ \qquad (3.11)

Comments: (1) The details of the derivation of eqn. (3.9) can be found in [6].

(2) Given any arbitrary neighbor set N, and the parameters $\theta_{i,j}$, $(i,j) \in N$, the correlation function at a specified lag can be computed easily.

We give below the computed correlation values for different neighbor sets and parameter values. The corresponding structure at lower lags is also given.

Case i: Semicausal simultaneous models

Consider the neighbor set $N = \{(1,0),(0,-1),(-1,0)\}$, corresponding to the model

$$y(s) - \delta = \sum_{(i,j) \in N} \theta_{i,j} [y(s+(i,j)-\delta] + \sqrt{v} w(s) \qquad (3.12)$$

The lower order correlations computed using (3.9) and the structure along each axis are given in Tables 1 and 2. The following observations are of significance:

1) For the isotropic case, for a range of parameters .31-.33, the ACF has a flat structure along the i-axis.

2) The ACF has a nonflat structure along the j-axis for the complete range of parameter values.

3) By making $\theta_{0,-1}$ as large as possible the actual correlation values $\rho(0,1), \rho(0,2)$ can be increased but the structure is still nonflat along the j-axis.

Case ii: Noncausal simultaneous models

Consider the neighbor set $N = \{(0,1),(1,0),(0,-1),(-1,0)\}$ corresponding to the RF model

$$y(s)-\delta = \sum_{(i,j) \in N} \theta_{i,j}[y(s+(i,j)-\delta]+\sqrt{\nu}\omega(s), \quad s \in \Omega \qquad (3.13)$$

The numerical values of the ACF and the structure at lower lags along the different axes are summarized in Tables 3 and 4. Table 3 corresponds to the isotropic case and Table 4 to the nonisotropic case. The following observations are of interest:

1) The ACF in the continuous case is flat in all directions. In the discrete case flat structure along the i,j and k axes is exhibited at values of θ close to .245 and above.

2) Flat structure along the i and j axes is exhibited for the range of parameters $\geq .2350$.

3) Introducing nonisotropy changes only the rate of decay of the correlation function, but the flat/nonflat behavior is unaltered.

Case iii: Noncausal 8-neighbor models

Consider the neighbor set $N = \{(0,1),(1,1),(1,0),(1,-1),(0,-1),(-1,-1),(-1,0),(-1,1)\}$ corresponding to the RF model

$$y(s)-\delta = \sum_{(i,j) \in N} \theta_{i,j}[y(s+(i,j))-\delta]+\sqrt{\nu}\omega(s), \quad s \in \Omega \qquad (3.14)$$

The numerical values and the structure at lower lags along
the different axes of the correlation function are tabulated in
Table 5. The relevant observations are:

1) For sufficiently high values of the parameters flat
structure is displayed along all axes.

2) By making different neighbors strong, flat structure can
be obtained along any desired axes.

3) For $\theta=.1220$, though the correlation values are high,
the structure is still nonflat along all axes.

3.3 Conditional Markov models on torus lattices

The basic equation of the conditional Markov model is

$$E(y(s) \mid \text{all } y(s_1), \ s_1 \in \Omega, \ s_1 \neq s) - \mu$$

$$= \sum_{(i,j) \in N_1} \theta_{i,j} [y(s+(i,j)) + y(s-(i,j)) - 2\mu] \qquad (3.15)$$

where N_1 is an appropriate neighbor set. Equivalently, (3.15) can be written as

$$y(s) - \mu = \sum_{(i,j) \in N_1} \theta_{i,j} [y(s+(i,j)) + y(s-(i,j)) - 2\mu] + \sqrt{v}\, e(s) \qquad (3.16)$$

where $\{e(s), \ s \in \Omega\}$ is a __correlated__ noise sequence with zero mean and unit variance. Note that a symmetric structure is imposed on the basic equation of a conditional RF model, i.e., when a neighbor (i,j) is included the neighbor $(-i,-j)$ is automatically included. Thus it is sufficient to characterize the neighbor set by using the set N_1, which includes only half of the symmetric neighbor set. Thus if the dependence is on the neighbors $\{(0,1),(1,0),(0,-1),(-1,0)\}$, we denote this by using the set $N_1 = \{(0,1),(1,0)\}$. For stationarity of $y(\cdot)$, the coefficients must satisfy the condition

$$\left| \sum_{(k,\ell) \in N_1} \theta_{k,\ell} (z_1^k z_2^\ell + z_1^{-k} z_2^{-\ell}) \right| < 1, \quad \text{when } |z_1| = |z_2| = 1 \qquad (3.17)$$

The representation on a torus lattice is obtained by imposing condition (3.8). This representation leads to the following expression for the ACF:

$$\rho(k,\ell) = \text{cov}[y(i_1,j_1), y(i_1+k, j_1+\ell)]$$

$$= \frac{\sum\limits_{i,j=1}^{M} \lambda_0 [(i-1)k + (j-1)\ell] / ||\mu'_{ij}||^2}{\sum\limits_{i,j=1}^{M} 1 / ||\mu'_{ij}||^2} \qquad (3.18)$$

where

$$\mu'_{ij} = 1+2 \sum_{(m,n) \in N_1} \cos \lambda_0 [(i-1)m+(j-1)n] \qquad (3.19)$$

and

$$\lambda_0 = \exp\{\sqrt{-1}\ \frac{2\pi}{m}\} \qquad (3.20)$$

Comments: The details of the derivation of (3.17) can be found in [6]. Given an arbitrary neighbor set N_1 and the parameters $\theta_{i,j}$, $(i,j) \in N_1$, the ACF at a specified lag can be computed easily.

We consider the computation of the ACF for some conditional models.

Case a: Noncausal conditional model

Consider the neighbor set $N_1 = \{(0,1),(1,0)\}$, corresponding to the RF model

$$y(s)-\mu = \theta_{0,1}[y(s+(0,1))+y(s+(0,-1))]$$
$$+ \theta_{1,0}[y(s+(1,0)+y(s+(-1,0))] + \sqrt{v}e(s) \qquad (3.21)$$

The lower order correlations and structure of ACF along the axes are given in Tables 6 and 7. Some of the interesting observations are:

1) The values of the correlation are much lower compared to the correlation values of simultaneous models in Tables 3 and 4. The ACF is monotonically decreasing and the $\rho(0,4)$, $\rho(4,0)$ (not shown in the table) are very close to 0.

2) Even at the high values of the parameter the ACF does not possess flat structure along any axis.

3) There is a tradeoff in the numerical values of the parameter and the correlation values. Even when the parameter is increased to .475 in Table 7, $\rho(0,1)$ is only 0.7673.

Case b: Noncausal conditional models

Consider the neighbor set $N_1 = \{(0,1),(1,0),(-1,1),(1,1)\}$, corresponding to the RF model

$$y(s)-\mu = \theta_{0,1}[y(s+(0,1))+y(s+(0,-1))]$$
$$+ \theta_{1,0}[y(s+(1,0))+y(s+(-1,0))]$$
$$+ \theta_{-1,1}[y(s+(-1,1))+y(s+(1,-1))]$$
$$+ \theta_{1,1}[y(s+(1,1))+y(s+(-1,-1))]$$
$$+\sqrt{v}e(s) \qquad\qquad (3.22)$$

The lower order correlations and the structure along the axes are tabulated in Table 8. The relevant observations are:

1) The correlation values are much lower compared to the simultaneous model with the same neighbor set.

2) The ACF always has nonflat structure (compare with Table 5).

3) The correlation values are higher when compared to the four-neighbor conditional model in (3.21).

3.4 Spatial moving average model

Moving average models have been found to be very useful in time series studies and hence their two-dimensional generalizations should also be useful in modeling the observations from a grid. The ACF of MA models falls off very rapidly. Specifically, the isotropic four-neighbor model considered here has zero correlation values beyond lag 2 and has nonflat structure along all directions.

Assume that the observations $\{y(s), s \in \Omega\}$ obey the MA model

$$y(i,j) = \theta(\omega(i-1,j)+\omega(i+1,j)+\omega(i,j-1)+\omega(i,j+1)+\omega(i,j)), |\theta| \leq \frac{1}{4}$$

(3.23)

where $\{\omega(i,j), (i,j) \in \Omega\}$ is an i.i.d. noise sequence. The two-dimensional spectral density function $S_y(\omega_1,\omega_2)$ is given by

$$S_y(\omega_1,\omega_2) = \sigma^2(1+2\theta\cos\omega_1+2\theta\cos\omega_2)^2$$

(3.24)

Using the Fourier relationship between the ACF and the spectral density function, the correlation function is

$$\rho(k,\ell) = \frac{1}{4(1+4\theta)^2} \frac{1}{\pi^2} \int_{-\pi}^{\pi} \int_{-\pi}^{\pi} \cos kw_1 \cos \ell w_2 (1+2\theta\cos w_1 + 2\theta\cos w_2)^2 dw_1 dw_2$$

(3.25)

Performing the integration in (3.25) to evaluate a few low order correlation values we obtain the results shown in Table 9.

It can be easily checked that the ACF has nonflat structure along all axes, in the allowed ranges of θ. The actual values of the correlations are tabulated in Table 10. The correlations

decay rapidly, and in fact the theoretical correlations $\rho(2,3)$, $\rho(3,3)$ are zero. The nearest correlations $\rho(1,0)=\rho(0,1)$ are bounded above by .4.

The above method of evaluating the ACF values becomes tedious for an isotropic MA model. However by considering the MA model on a torus lattice closed form expressions can be obtained for the ACF.

Assume that the observations obey the MA model in (3.26) and the torus conditions in (3.8):

$$y(s) = \Sigma\theta_{i,j}\omega(s+(i,j))+\omega(s), \quad s\in\Omega \tag{3.26}$$

To ensure stationarity the following condition should be satisfied:

$$\left|\sum_{(i,j)\in N}\theta_{i,j}z_1^i z_2^j\right| < 1 \quad \text{if } |z_1|=|z_2|=1$$

where N is the neighbor set of dependence.

The torus representation for MA models leads to the following expression for the ACF:

$$\rho(k,\ell) = \frac{\sum_{i,j=1}^{m}\lambda_0[(\rho-1)k+(j-1)\ell]\,||\mu_{ij}||^2}{\sum_{i,j=1}^{m}||\mu_{ij}||^2} \tag{3.27}$$

where

$$\mu_{ij} = 1+\sum_{(m,n)\in N}\theta_{m,n}\lambda_0[(i-1)m+(j-1)n] \tag{3.28}$$

and

$$\lambda_0 = \exp\{\sqrt{-1}\frac{2\pi}{m}\} \tag{3.29}$$

The derivation of (3.27) is given in the appendix.

The ACF values computed using (3.27) and N={(0,1),(1,0),
(0,-1),(-1,0)} are given in Table 11. Note that the ACF values
are slightly different (see the row corresponding to $\theta = .24$)
from the exact values in Table 10. This is due to the torus
assumption introduced. However the error due to the approxima-
tion is negligible.

3.5 Spatial autoregressive and moving average models

For the sake of completeness we consider the correlation structure of spatial ARMA models. We assume that the given observations $\{y(s), s \in \Omega\}$ obey the RF model

$$y(s) = \sum_{(i,j) \in N} \theta_{i,j} y(s+(i,j)) + \sum_{(i,j) \in N} \beta_{i,j} \omega(s+(i,j))$$

$$+ \sqrt{\nu} \omega(s) \tag{3.30}$$

To ensure stationarity the following condition should be satisfied:

$$\left| \sum_{(i,j) \in N} \theta_{i,j} z_1^i z_2^j \right| < 1$$

and

$$\left| \sum_{(i,j) \in N} \beta_{i,j} z_1^i z_2^j \right| < 1 \quad \text{whenever} \quad |z_1| = |z_2| = 1$$

The torus representation leads to the following expression for the ACF:

$$\rho(k,\ell) = \frac{\sum_{i,j=1}^{m} \lambda_0 [(i-1)k+(j-1)\ell] \, ||\mu'_{ij}||^2 / ||\mu_{ij}||^2}{\sum_{i,j=1}^{m} ||\mu'_{ij}||^2 / ||\mu_{ij}||^2} \tag{3.31}$$

where

$$\mu'_{i,j} = 1 + \sum_{(m,n) \in N} \theta_{m,n} \lambda_0 [(i-1)m+(j-1)n] \tag{3.32}$$

and

$$\mu_{ij} = 1 - \sum_{(m,n) \in N} \theta_{m,n} \lambda_0 [(i-1)m+(j-1)n] \tag{3.33}$$

Equation (3.33) can be derived similarly to (3.27) and is not given here. The ACF values computed for some parameter values in the allowed region are given in Table 12.

4. Experimental results

In the previous sections the correlation structure was analyzed for the different models. To determine if this structure matches with real data, experiments were done using 64x64 windows from real image patterns. Four windows, each from four Brodatz textures, sand, wool, grass, and raffia, and from three terrain textures, lower Pennsylvanian shale (LP), Mississippian limestone and shale (ML), and Pennsylvanian sandstone and shale (PS), were used in the experiments. The sample correlation function, r(s,t), defined below was computed for each window.

$$r(s,t) = \frac{1}{(N-s)(N-t)} \cdot \frac{\sum\limits_{i=1}^{N-s} \sum\limits_{j=1}^{N-t} (y(i,j)-\hat{\mu})(y(i+s,j+t)-\hat{\mu})}{\frac{1}{N^2} \sum\limits_{i=1}^{N} \sum\limits_{j=1}^{N} (y(i,j)-\hat{\mu})^2} \qquad (4.1)$$

where $\hat{\mu} = \frac{1}{N^2} \sum\limits_{i=1}^{N} \sum\limits_{j=1}^{N} y(i,j)$ \qquad (4.2)

The computed sample ACFs for the Brodatz textures and the terrain samples and the corresponding correlation structures are given in Tables 13 and 14.

By matching the sample correlation structures and the theoretical correlation structures useful inferences may be drawn about the types of models that are appropriate for given images. Consider, for instance, the windows of the Brodatz sand texture.

The correlation functions exhibit flat structure along all axes and the correlation values are quite high. Noncausal simultaneous models with neighbor sets (east, west, north, and south) or (east, west, north, south and the four diagonal neighbors) seem appropriate, since the causal and seimcausal simultaneous models, the conditional Markov models, and the MA models do not have flat structure along all axes. Similar conclusions can be drawn for the grass and wool textures. All the windows from raffia have flat structure along the i and j axes and nonflat structure along the k-axis. The noncausal simultaneous models in (3.13) possess this structure for some ranges of parameter values. By manipulating the parameter corresponding to different neighbors the RF model in (3.14) can be made to have this structure.

The windows of terrain types LP and ML have nonflat structure along all axes and the correlation values are quite low. For these windows, the causal, semicausal, and noncausal simultaneous models and the conditional Markov models can be considered. Since some of the windows (2 and 4 of LP) have nearly equal values of $\rho(1,0)$ and $\rho(0,1)$, the semicausal models can be dropped out of consideration.

The windows of terrain type PS exhibit flat structure along the i axis and nonflat structure along the j and k axes. The semicausal and noncausal simultaneous models in equation (3.12) and (3.16) possess this structure (see Tables 1, 2, and 5).

As another illustration consider the classical Mercer and Hall wheat data mentioned in [3]. The data presents the results of a uniformity trial on wheat. The ACF values of this data at lower lags is given in Table 15 (taken from [3]) together with the structure along each axis. Since the structure is nonflat along all axes, our inference method suggests that it is appropriate to consider the causal simultaneous models, conditional Markov models, and MA models. The MA models can be avoided since the ACF has large values at lags of 3 and 4. So the choice is between causal simultaneous models and conditional models. Our conclusion that causal simultaneous models are preferable to noncausal simultaneous models agrees with Whittle's observation [3], that unilateral models fit better than the noncausal models. The final choice between the conditional models and the simultaneous models can be made by using the theory developed in [1] and [6].

5. Discussion

We have considered the correlation structure of some NNRF models. Specifically, we considered two classes of RF models, simultaneous models and conditional Markov models. We make a brief comparison of the models below.

Of the 4-neighbor noncausal simultaneous models (3.13) and the conditional Markov models (3.21) the former always account for higher correlations than the latter. Also, the simultaneous models exhibit a different structure (which is observed in some real textures) that is not possessed by the conditional Markov models. Even when the neighbor set is as in (3.22) (four more diagonal neighbors added), the correlation values are lower (Table 8) compared to the simultaneous model with four neighbors (Tables 3 and 4). To account for the same correlations as in a 4-neighbor non-isotropic simultaneous model, a conditional model which includes the nearest neighbors and 4 additional neighbors on the east, west, north, and south is required [4]. This necessitates the use of a 6-parameter model. One of the well-known rules in model building is to keep the parameters to a minimum. Thus, the simultaneous model with 4 neighbors is preferable to the conditional model with 6 parameters.

Secondly, the conditional models defined by the conditional probability structure (3.15) are subject to some unobvious and highly restrictive consistency conditions. When these conditions are enforced, the conditional probability structure becomes

degenerate [14] with respect to the joint probability structure implicit in the definition of simultaneous models.

Thirdly, the reflection-symmetric condition on the parameters of the conditional Markov model is not required in the simultaneous models.

The conditional models with 4 neighbors have correlation values between those of the simultaneous models and MA models with the same neighbor sets. The MA models have a rapidly decaying ACF, and are appropriate for patterns which have strong local dependence.

The possible structures of the ACF that can be accounted for by the simultaneous models are quite varied compared to the conditional models (see Tables 3, 4, and 5). The particular flat structure observed in the simultaneous models is due to the bilateral dependence introduced. When the neighbor set {(0, 1), (0,-1), (-1,0)} is considered, flat structure only along the j axis is observed (not tabulated here) for ranges of parameter values. A similar behavior is shown in Table 5, where by making particular neighbors strong (high parameter value), flat structure along the desired axis is obtained. [For no explicable reasons, the neighbors {(-1,1), (+1,-1)} do not contribute to the flat structure along any axis.] Note that the causal separable simultaneous model does not possess flat structure throughout the allowed ranges of the parameter values. Also, in the semicausal simultaneous model, the structure is

always nonflat along the j axis. The 4-neighbor set conditional Markov models also possess nonflat structure along all axes as their continuous counterparts suggest.

The empirical inference method discussed in this paper for identifying the models is not necessarily exact. It is inexact, because the question of what types of models occur in practice and in what circumstances, is a property of the behavior of the physical world and cannot be decided by purely analytical argument. However, the preliminary identification commits us to nothing except to tentatively entertaining a class of plausible models.

The analysis of ACF structure undertaken here is relevant to studies of texture. It is known that the rate of falloff of the ACF is related to the size of tonal primitives [15]. If the tonal primitives are relatively large, the ACF drops slowly, while if the tonal primitives are small, the ACF drops quickly. Also, it is known that tonal primitives of larger size are indicative of coarser textures and tonal primitives of smaller size are indicative of finer textures. It has been experimentally verified that there is a very high positive correspondence [16] between the grading of textures from fine to coarse by human viewers and the $\frac{1}{e}$ distance of the ACF. Thus, the usefulness of the ACF as an inference tool need not be overemphasized.

References

1. R. L. Kashyap, R. Chellappa, and N. Ahuja, "Decision rules for the choice of neighbors in random field models of images" (to appear).

2. G. E. P. Box and G. M. Jenkins, Time Series Analysis - Forecasting and Control, Holden-Day, San Francisco, California, 1976.

3. P. Whittle, "On stationary processes in the plane," Biometrika, vol. 41, pp. 434-449, 1954.

4. M. S. Bartlett, The Statistical Analysis of Spatial Patterns, Chapman and Hall, London, 1975.

5. R. L. Kashyap, "Univariate and multivariate random field models for images," Computer Graphics and Image Processing, vol. 12, pp. 257-270, 1980.

6. R. L. Kashyap, "Random field models on torus lattices for finite images" (submitted).

7. M. Hassner and J. Sklansky, "Markov random field models of digitized image textures," Computer Graphics and Image Processing, vol. 12, pp. 357-370, 1980.

8. J. E. Besag, "On the correlation structure of some two-dimensional stationary processes," Biometrika, vol. 59, pp. 43-58, 1972.

9. P. Whittle, "Stochastic processes in several dimensions," Bull. Int. Stat. Inst., vol. 40, pp. 974-994, 1963.

10. A. K. Jain, "Partial differential equations and finite differences in image processing, part 1 - image representation," J. Optimiz. Theory and Appl., vol. 23, pp. 65-91, 1977.

11. I. N. Sneddon, Elements of Partial Differential Equations, McGraw Hill, New York, 1957.

12. V. Heine, "Models for two-dimensional stationary stochastic processes," Biometrika, vol. 42, pp. 170-178, 1955.

13. A. Rosenfeld and A. C. Kak, Digital Picture Processing, Academic Press, New York, 1976.

14. D. Brook, "On the distinction between the conditional probability and the joint probability approaches for the specification of nearest-neighbor systems," Biometrika, vol. 51, pp. 481-483, 1964.

15. R. M. Haralick, "Statistical and structural approaches to texture," _Proc. IEEE_, vol. 67, pp. 786-804, 1979.

16. H. Kaizer, "A quantification of textures on aerial photographs," Boston University Research Laboratories, Technical Note 121, 1955, AD69484.

Appendix

We derive equation (3.27). Equation (3.26) can be equivalently written as

$$\underset{\sim}{y} = \sqrt{\nu} B(\theta) \underset{\sim}{\omega} \tag{1}$$

where $y^T = \{y(1,1), y(1,2),\ldots,y(1,M),\ldots,y(M,1),\ldots,y(M,M)\}$,
$\omega^T = \{\omega(1,1),\ldots,\omega(M,M)\}$ and $B(\theta)$ is a block circulant matrix

$$B = \begin{bmatrix} B_{1,1} & B_{1,2} & \cdots & B_{1,M} \\ B_{1,M} & B_{1,1} & \cdots & B_{1,M-1} \\ \cdots & \cdots & \cdots & \cdots \\ B_{1,2} & B_{1,3} & \cdots & B_{1,1} \end{bmatrix} \tag{2}$$

For example, when $N = \{(0,1),(1,0),(0,-1),(-1,0)\}$, we have

$$B_{1,1} = \text{circulant}\ (1,\theta_{0,1},0,\ldots,\theta_{0,-1})$$
$$B_{1,2} = \text{circulant}(\theta_{1,0},0,\ldots,0)$$
$$B_{1,M} = \text{circulant}\ (\theta_{-1,0},0,\ldots,0)$$
$$B_{1,j} = 0 \qquad j \neq 1,2,M$$

Hence the covariance matrix $Q = E(\underset{\sim}{y}\underset{\sim}{y}^T)$ can be written as

$$\underset{\sim}{Q} = B(\theta)B^T(\theta) \tag{3}$$

From the theory of circulant matrices, the eigenvectors of $B(\theta)$ are the Fourier vectors $\underset{\sim}{f}_{ij}$, $1 \leq i, j \leq M$ where

$$\underset{\sim}{f}_{ij} = \text{column}(\underset{\sim}{t}_j, \lambda_i \underset{\sim}{t}_j, \ldots, \lambda_i^{M-1} \underset{\sim}{t}_j)$$
$$\underset{\sim}{t}_j = \text{column}(1, \lambda_j, \lambda_j^2, \ldots, \lambda_j^{M-1})$$

and $\lambda_i = \lambda_0(i-1)$

and the corresponding eigenvectors are

μ_{ij}, $1 \le i, j \le M$ defined as

$$\mu_{ij} = 1 + \sum_{(m,n) \in N} \theta_{m,n} \{\lambda_0 [(i-1)m + (j-1)n]\} \qquad (4)$$

Since $\underset{\sim}{Q}$ is a symmetric block-circulant matrix, $\underset{\sim}{Q}$ can be expanded in terms of its eigenvectors as

$$\underset{\sim}{Q} = \frac{1}{M^2} \sum_{i,j=1}^{M} \underset{\sim}{f}_{ij} \underset{\sim}{f}_{ij}^{*T} ||\mu_{ij}||^2 \qquad (5)$$

Using (5) and the definition of $\rho(k,\ell)$

$$\rho(k,\ell) = \frac{q_{M(i_1-1)+j_1, M(i_1+k-1)+j_1+\ell-1}}{q_{M(i_1-1)+j_1, M(i_1-1)+j_1}}$$

where $q_{i,j}$ denotes the (i,j)th element of $\underset{\sim}{Q}$, we arrive at (3.27).

Value of	c(1,0)	c(2,0)	c(0,1)	c(0,2)	c(1,1)	c(2,2)	Structure along axes		
							i	j	k
.18	.3733	.1078	.2207	.0503	.1144	.0143	NF	NF	NF
.22	.4678	.1735	.3024	.0974	.1885	.0387	NF	NF	NF
.26	.5747	.2706	.4165	.1871	.3020	.0983	NF	NF	NF
.30	.7108	.4367	.5970	.3835	.4958	.2593	NF	NF	NF
.31	.7561	.5042	.6636	.4709	.5709	.3407	F	NF	NF
.32	.8128	.5990	.7487	.5928	.6704	.4642	F	NF	NF
.35	.9138	.7988	.8931	.8214	.8514	.7357	F	NF	NF

Table 1. ACF of isotropic semicausal neighbor set {(1,0),(0,1),(0,-1),(-1,0)}.
c(0,0)≡1. NF: nonflat structure. F: flat structure.

Value of parameter			ρ(1,0)	ρ(2,0)	ρ(0,1)	ρ(0,2)	ρ(1,1)	ρ(2,2)	Structure along axes		
$\theta_{1,0}$	$\theta_{0,-1}$	$\theta_{-1,0}$							i	j	k
.45	.09	.45	.9546	.8710	.7681	.6228	.7535	.5941	F	NF	NF
.4	.19	.4	.9334	.8290	.8446	.7430	.8181	.6880	F	NF	NF
.18	.60	.18	.6922	.4427	.8313	.7105	.6428	.4143	NF	NF	NF
.02	.92	.02	.3056	.0968	.9341	.8735	.3037	.0968	NF	NF	NF
.55	.32	.11	.8681	.7301	.7797	.6149	.6782	.4485	F	NF	NF
.05	.32	.60	.8379	.6894	.7165	.5157	.7326	.5946	NF	NF	NF

Table 2. ACF of non-isotropic semicausal neighbor set $\{(1,0),(0,-1),(-1,0)\}$.

Parameter ρ	$c(1,0)$ $=c(0,1)$	$c(2,0)$ $=c(0,2)$	$c(1,1)$	$c(2,2)$	Structure along axes		
					i	j	k
.1	.2124	.0342	.0650	.0035	NF	NF	NF
.14	.3186	.0797	.1398	.0162	NF	NF	NF
.18	.4556	.1700	.2670	.0597	NF	NF	NF
.22	.6631	.3825	.5080	.2216	NF	NF	NF
.23	.7396	.4870	.6086	.3230	NF	NF	NF
.235	.7852	.5571	.6714	.3977	F	F	NF
.24	.8383	.6464	.7472	.5010	F	F	NF
.245	.9034	.7705	.8440	.6574	F	F	F

Table 3. ACF of isotropic noncausal neighbor set $\{(0,1),(1,0),(0,-1),(-1,0)\}$.

| Parameter | | | | $\rho(1,0)$ | $\rho(2,0)$ | $\rho(0,1)$ | $\rho(0,2)$ | $\rho(1,1)$ | $\rho(2,2)$ | Structure along axes | | |
$\theta_{0,1}$	$\theta_{1,0}$	$\theta_{0,-1}$	$\theta_{-1,0}$							i	j	k
.2686	.2173	.2686	.2173	.8638	.6943	.8843	.7311	.7993	.5815	F	F	F
.1179	.3830	.1179	.3880	.9920	.9709	.9613	.8586	.9544	.8347	F	F	F
.1	.25	.2	.4	.8412	.6515	.7219	.4808	.6740	.4325	F	NF	NF
.8	.04	.04	.04	.2925	.0789	.8620	.7361	.2832	.0775	NF	NF	NF
.4	.15	.3	.1	.7028	.4467	.8604	.6794	.6572	.3928	NF	F	NF
.4	.02	.3	.25	.7651	.6004	.8633	.6871	.6930	.4701	F	F	NF
.15	.3	.1	.35	.7740	.5270	.5771	.2938	.5021	.2173	NF	NF	NF

Table 4. ACF of non-isotropic noncausal neighbor set $\{(0,1),(1,0),(0,-1),(-1,0)\}$.

Parameter	$\rho(1,0)$	$\rho(2,0)$	$\rho(0,1)$	$\rho(0,2)$	$\rho(1,1)$	$\rho(2,2)$	Structure along axes		
							i	j	k
Isotropic: $\theta=.1220$	.8773	.7657	.8713	.7657	.8419	.6730	NF	NF	NF
Isotropic: $\theta=.1240$	.9508	.8954	.9508	.8954	.9329	.8432	F	F	F
$\theta_{-1,0}=\theta_{1,0}=-.35$, other coefficients =.04	.8510	.6663	.6419	.3825	.6085	.3332	F	NF	NF
$\theta_{1,1}=\theta_{-1,-1}=.35$, other coefficients =.04	.5995	.4449	.5995	.4449	.8285	.6227	NF	NF	F
$\theta_{0,1}=\theta_{0,-1}=.35$, other coefficients =.04	.6419	.3825	.8510	.6663	.6085	.3332	NF	F	NF
$\theta_{-1,1}=\theta_{1,-1}=.35$, other coefficients=.04	.5995	.4449	.5995	.4449	.4755	.2100	NF	NF	NF

Table 5. ACF for the noncausal simultaneous model in (3.14).

Parameter	$\rho(1,0)$ $=\rho(0,1)$	$\rho(2,0)$ $=\rho(0,2)$	$\rho(1,1)$	$\rho(2,2)$	Structure along axes		
					i	j	k
.1	.1049	.0107	.0217	.0007	NF	NF	NF
.14	.1561	.0249	.0467	.0033	NF	NF	NF
.18	.2215	.0523	.0904	.0122	NF	NF	NF
.22	.3251	.1187	.1804	.0482	NF	NF	NF
.23	.3680	.1547	.2234	.0736	NF	NF	NF
.24	.4329	.2181	.2935	.1254	NF	NF	NF
.245	.4884	.2803	.3572	.1828	NF	NF	NF
.2499	.7007	.5658	.6193	.4941	NF	NF	NF

Table 6. ACF values for the isotropic, noncausal conditional model in (3.20).

| Parameter | | $\rho(1,0)$ | $c(2,0)$ | $\rho(0,1)$ | $\rho(0,2)$ | $\rho(1,1)$ | $c(2,2)$ | Structure along axes | | |
$\theta_{0,1}$ $=\theta_{0,-1}$	$\theta_{1,0}$ $=\theta_{-1,0}$							i	j	k
.475	.02	.2623	.0982	.7673	.5943	.2532	.0940	NF	NF	NF
.425	.07	.3862	.2011	.6796	.4823	.3557	.1814	NF	NF	NF
.393	.087	.2890	.1100	.5677	.3366	.2452	.0883	NF	NF	NF
.368	.107	.2939	.1111	.5262	.2923	.1706	.0933	NF	NF	NF

Table 7. ACF values of the nonisotropic, noncausal conditional Markov model in (3.20).

Parameter	$\rho(1,0)$	$\rho(2,0)$	$\rho(0,1)$	$\rho(0,2)$	$\rho(1,1)$	$\rho(2,2)$	Structure along axes		
							i	j	k
Isotropic: $\theta=.1220$	.3850	.2427	.3850	.2427	.3510	.1779	NF	NF	NF
Isotropic: $\theta=.1240$	.4591	.3253	.4591	.3253	.4262	.2595	NF	NF	NF
$\theta_{1,0}=.35$, other coefficients $=.04$	.4929	.2646	.2465	.0945	.2235	.0755	NF	NF	NF
$\theta_{1,1}=.35$, other coefficients $=.04$	.2063	.1227	.2063	.1227	.4716	.2371	NF	NF	NF
$\theta_{0,1}=.35$, other coefficients $=.04$	.2465	.0945	.4929	.2646	.2235	.0755	NF	NF	NF
$\theta_{-1,1}=.35$, other coefficients $=.04$	.2063	.1227	.2063	.1227	.1492	.0380	NF	NF	NF

Table 8. ACF for the noncausal conditional Markov model in (3.22).

$$\ell$$

		0	1	2
k	0	1	$2k\theta$	$k\theta^2$
	1	$2k\theta$	$2k\theta^2$	0
	2	$k\theta^2$	0	0

where $k = (1+4\theta^2)^{-1}$

Table 9. Lower order correlations of moving average model
         in (3.23).

Parameter	$\rho(1,0)$ $=\rho(0,1)$	$\rho(2,0)$ $=\rho(0,2)$	$\rho(1,1)$	$\rho(2,2)$	Structure along axes		
					i	j	k
.1000	.1923	.0096	.0192	0.00	NF	NF	NF
.1400	.2596	.0182	.0364	0.00	NF	NF	NF
.1800	.3187	.0287	.0574	0.00	NF	NF	NF
.2200	.3686	.0405	.0811	0.00	NF	NF	NF
.2400	.3901	.0468	.0936	0.00	NF	NF	NF
.2499	.3999	.0500	.0999	0.00	NF	NF	NF

Table 10. ACF for the moving average model in (3.23).

| Parameter | | | | $\rho(1,0)$ | $\rho(2,0)$ | $\rho(0,1)$ | $\rho(0,2)$ | $\rho(1,1)$ | $\rho(2,2)$ | Structure along axes | | |
$\theta_{0,1}$	$\theta_{1,0}$	$\theta_{0,-1}$	$\theta_{-1,0}$							i	j	k
.24	.24	.24	.24	.3896	.0459	.3896	.0459	.0924	.0000	NF	NF	NF
.12	.34	.12	.34	.5392	.0909	.1900	.0107	.0644	.0001	NF	NF	NF
.11	.21	.16	.48	.5251	.0758	.2052	.0127	.0655	.0000	NF	NF	NF
.22	.12	.13	.23	.3085	.0236	.3085	.0244	.0581	.0000	NF	NF	NF

Table 11. ACF values for MA model on torus lattice for the neighbor set
$N = \{(0,1),(1,0),(0,-1),(-1,0)\}$

Parameters	$\rho(1,0)$	$\rho(2,0)$	$\rho(0,1)$	$\rho(0,2)$	$\rho(1,1)$	$\rho(2,2)$	Structure along axes		
							i	j	k
$\theta_{0,1}=\theta_{1,0}=\theta_{0,-1}=\theta_{-1,0}=.24$ $\beta_{0,1}=\beta_{1,0}=\beta_{0,-1}=\beta_{-1,0}=.24$	.8046	.7250	.9046	.7250	.8278	.5719	F	F	F
$\theta_{0,1}=-.14,\ \theta_{1,0}=.18$ $\theta_{0,-1}=-.24,\ \theta_{-1,0}=.32$ $\beta_{0,1}=.22,\ \beta_{1,0}=-.12$ $\beta_{0,-1}=-.16,\ \beta_{-1,0}=.24$	.8046	.5250	.7663	.4570	.6476	.3185	F	F	NF
$\theta_{0,1}=\theta_{1,0}=\theta_{0,-1}=\theta_{-1,0}=.04$ $\beta_{0,1}=\beta_{1,0}=\beta_{0,-1}=\beta_{-1,0}=.24$	.4413	.0750	.4413	.0750	.1489	.0017	NF	NF	NF

Table 12. ACF values for ARMA model on torus lattice for the neighbor set
$N=N'=\{(0,1),(1,0),(0,-1),(-1,0)\}$

Texture	WINDOW	r(1,0)	r(2,0)	r(0,1)	r(0,2)	r(1,1)	r(2,2)	Structure along i-axis	Structure along j-axis	Structure along i-axis
SAND	1	.893	.676	.926	.764	.852	.608	F	F	F
	2	.924	.752	.925	.749	.896	.682	F	F	F
	3	.897	.690	.883	.662	.833	.555	F	F	F
	4	.852	.588	.896	.676	.799	.495	F	F	F
GRASS	1	.839	.550	.909	.709	.802	.498	F	F	F
	2	.848	.569	.896	.672	.807	.508	F	F	F
	3	.838	.521	.890	.672	.768	.396	F	F	F
	4	.875	.639	.911	.730	.837	.571	F	F	F
RAFFIA	1	.719	.389	.637	.239	.508	.061	F	F	NF
	2	.718	.377	.643	.244	.492	.056	F	F	NF
	3	.716	.393	.631	.198	.514	.053	F	F	NF
	4	.736	.425	.596	.121	.488	.003	F	F	NF
WOOL	1	.883	.719	.941	.832	.843	.637	F	F	F
	2	.905	.737	.907	.731	.831	.564	F	F	F
	3	.905	.737	.894	.733	.812	.569	F	F	F
	4	.906	.712	.895	.720	.812	.533	F	F	F

Table 13. Sample estimates of ACF for Brodatz textures.

Texture	WINDOW	r(1,0)	r(2,0)	r(0,1)	r(0,2)	r(1,1)	r(2,2)	Structure along i-axis	Structure along j-axis	Structure along k-axis
LP	1	.562	.147	.541	.249	.363	.096	NF	NF	NF
	2	.669	.296	.635	.352	.515	.250	NF	NF	NF
	3	.490	.191	.543	.241	.350	.090	NF	NF	NF
	4	.571	.125	.572	.282	.436	.162	NF	NF	NF
ML	1	.609	.228	.525	.242	.413	.148	NF	NF	NF
	2	.590	.207	.563	.292	.393	.148	NF	NF	NF
	3	.607	.200	.529	.245	.407	.147	NF	NF	NF
	4	.593	.196	.467	.177	.335	.114	NF	NF	NF
PS	1	.729	.362	.699	.436	.585	.289	F	NF	NF
	2	.681	.261	.722	.461	.573	.265	F	NF	NF
	3	.786	.510	.764	.555	.668	.462	F	NF	NF
	4	.737	.348	.744	.502	.630	.326	F	NF	NF

Table 14. Sample estimates of ACF for terrain samples.

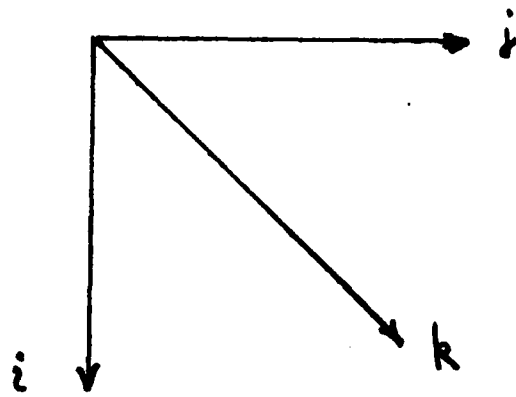|						Structure along axes		
r(1,0)	r(2,0)	r(0,1)	r(0,2)	r(1,1)	r(2,2)	i	j	k
.5252	.4055	.2923	.1510	.2354	.0999	NF	NF	NF
						NF	NF	NF

Table 15. ACF structure of Mercer and Hall wheat data [3].

Fig. 1   Convention for co-ordinate axes.